Vrije Universiteit Brussel

Miniaturized broadband spectrometer based on a three-segment diffraction grating for spectral tissue sensing

Belay, Gebirie Yizengaw; Hoving, Willem; van der Put, Arthur ; Vervaeke, Michael; Van Erps, Jürgen; Thienpont, Hugo; Ottevaere, Prof. Dr. Ir. Heidi

Published in:
Optics and Lasers in Engineering

DOI:
10.1016/j.optlaseng.2020.106157

Publication date:
2020

License:
CC BY-NC-ND

Document Version:
Accepted author manuscript

Link to publication

Citation for published version (APA):
Belay, G. Y., Hoving, W., van der Put, A., Vervaeke, M., Van Erps, J., Thienpont, H., & Ottevaere, P. D. I. H. (2020). Miniaturized broadband spectrometer based on a three-segment diffraction grating for spectral tissue sensing. *Optics and Lasers in Engineering*, *134*, 1-9. [106157]. https://doi.org/10.1016/j.optlaseng.2020.106157

Copyright
No part of this publication may be reproduced or transmitted in any form, without the prior written permission of the author(s) or other rights holders to whom publication rights have been transferred, unless permitted by a license attached to the publication (a Creative Commons license or other), or unless exceptions to copyright law apply.

Take down policy
If you believe that this document infringes your copyright or other rights, please contact openaccess@vub.be, with details of the nature of the infringement. We will investigate the claim and if justified, we will take the appropriate steps.

Download date: 19. Apr. 2024

Miniaturized broadband spectrometer based on a three-segment diffraction grating for spectral tissue sensing

Gebirie Yizengaw Belay[a*], Willem Hoving[b], Arthur van der Put[b], Michael Vervaeke[a], Jürgen Van Erps[a], Hugo Thienpont[a], Heidi Ottevaere[a]

[a] *Vrije Universiteit Brussel and FlandersMake, Faculty of Engineering, Dept. of Applied Physics and Photonics (TONA), Brussels Photonics (B-PHOT), Pleinlaan 2, B-1050 Brussel, Belgium*

[b] *Anteryon B.V., BIC 1, 5657 BX Eindhoven, The Netherlands*

**gizengaw@b-phot.org*

Abstract

Compact and broadband spectrometers are very useful in various application domains such as agriculture, food, health and security. In minimally-invasive image-guided procedures spectral tissue sensing helps for screening and diagnostic purposes aiming at discriminating between healthy and tumorous tissue at point-of-care locations and outpatient centers. We designed a compact spectrometer based on a three-segment diffraction grating which operates from 300 nm to 1700 nm. The first two segments of the grating cover spectral ranges from ultraviolet to visible and near infrared (UV, VIS/NIR), whereas the third segment covers the short-wave infrared (SWIR) region from 830 nm to 1700 nm. The spectrometer has a resolution of 6 nm in the UV-VIS/NIR ranges and 10 nm in the SWIR range. The smallest signal-to-noise ratio (SNR) of the spectrometer achieved in the VIS range is 650 and in the SWIR range 9300. Afterwards, the designed three-segment grating was fabricated in-house with ultra-precision diamond tooling followed by hot embossing and quantitatively characterized. The experimental results show that the three-segment grating improves the diffraction efficiency in the NIR-SWIR wavelength range by at least a factor of 2 compared to a Richardson grating which only operates from 300 nm to 1100nm. This result paves the way towards a new approach for making compact and low-cost spectrometers which could be integrated with hand held devices such as tablets and smartphones.

Key words: Three-segment diffraction grating, broadband spectrometer, spectral tissue sensing, VIS-NIR-SWIR spectrometer, open-arms Fastie-Ebert configuration, diffraction efficiency

1. Introduction

Minimally-invasive image-guided procedures are becoming increasingly important in clinical practice. In a variety of procedures physicians lack reliable feedback on the type of tissue at the tip of their interventional device (needle, catheter, endoscopic or laparoscopic probes, etc.…) to ensure they are at the right position before effecting the actual diagnosis or treatment and taking biopsy. Spectral tissue sensing using compact photonic probes has the promise to be a valuable tool for screening and diagnostic purposes, e.g. for discriminating between healthy and tumorous tissue. Real-time tissue characterization feedback to the physician during an intervention can significantly improve the outcome of a diagnosis and treatment, and ultimately reduces the cost of the medical treatment [1-5]. Diagnostics by means of spectral sensing is being used in a variety of point-of-care healthcare applications, such as photoplethysmography

(PPG) sensors, capnometers and pulse oximeters. It can also be used for detection purposes, for example, for the detection of skin melanoma [6], for localizing tumors using fluorescent markers [7], or for the detection of tumor margins during surgery [8]. Spectral tissue sensing, and screening rely on spectroscopic monitoring of a wide wavelength range, simultaneously covering both the visible and infrared part of the spectrum. Since spectral fingerprints of many molecules relevant for diagnostics and screening extend towards the shortwave-infrared, spectroscopic instruments are required that are capable of measuring the full UV, visible, near-infrared and shortwave-infrared region of the electromagnetic spectrum. Nowadays the major clinical trend is the gradual transition of screening, diagnosis and treatment from hospital to a point-of-care setting. Where traditionally screening and diagnostics was always performed within the radiology department, in the future mobile, cost-effective imaging and sensing solutions will enable physicians outside of the radiology department to diagnose and treat at the patient's bedside, in the general practitioners' office or day-clinics, or even in a home setting. This will enable earlier detection of diseases and treatment outside of expensive clinical infrastructures and thus reduce the overall financial burden on the healthcare system [9]. However, here, the enabling factor is the availability of small, affordable and easy to use devices.

The concept of a spectral tissue sensing device is shown in Figure 1. The device contains an optical fiber for broadband light delivery towards the tissue under study and collection and transport of scattered light from the tissue towards a measurement console. Today the measurement console contains a set of spectrometers capable of analyzing the scattered light in the 300-1700 nm spectral range. From these diffuse reflectance spectra, one is able to derive physiological parameters like e.g. blood, oxygenation and lipid content of the tissue that is in contact with the photonics needle, giving real-time feedback of the tissue characteristics to the physician during the intervention. In order to properly quantify these different tissue parameters, the UV, VIS/NIR as well as the SWIR parts of the spectrum are needed because they contain important molecular fingerprints that need to be subsequently recorded [10]. To differentiate a healthy tissue from a tumorous tissue, high sensitivity and specificity levels are required. Therefore, spectral tissue sensing applications require a minimum threshold of spectral resolution and signal-to-noise-ratio (SNR) of the device. For a good functional device, a resolution of 6 nm and 10 nm, and an SNR of 50 and 150 are required in the VIS-NIR and SWIR wavelength regions, respectively [11,12]. The spectral sensing technology is being investigated for real-time tissue characterization feedback in image guided procedures such as nerve detection in anesthesiology and as biopsy guidance in oncology. However, it can also be used for several other applications, e.g. food quality monitoring, agriculture, industrial inspection, etc.

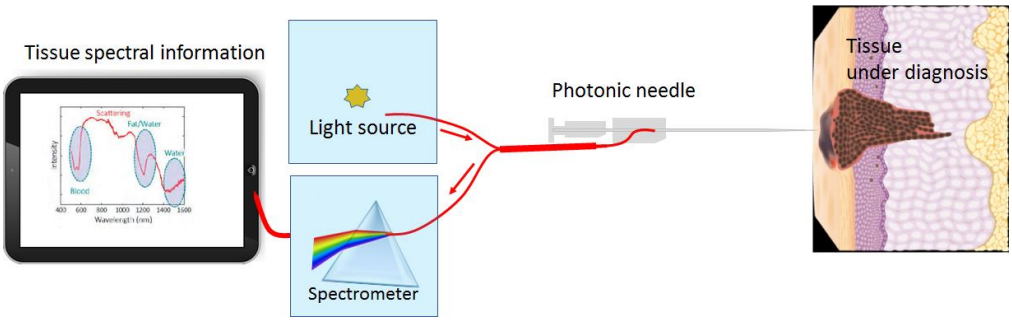

Figure 1. Spectral tissue sensing device, providing real-time feedback on tissue type, blood oxygenation, etc. to a physician [13].

For a widespread use of spectral tissue sensing, broadband miniature spectrometer devices should become available at affordable cost, to make it commercially viable for also screening at point-of-care locations such as physicians' offices and outpatient centers. Therefore, the goal of our research is to develop highly-integrated portable spectral-sensing devices covering a broad spectral range across the visible/near-infrared and shortwave-infrared (UV-VIS/NIR-SWIR, 300-1700nm) part of the spectrum with state-of-the-art specifications [13].

This paper is structured as follows. Section 2 describes our approach towards designing a miniature spectrometer and reviews the current state-of-the-art of compact spectrometers available on the market. The modelling and design of the miniature spectrometer is explained in section 3. Section 4 is dedicated to the sensitivity and irradiance analysis of the designed miniature spectrometer. Fabrication and characterization of the three-segment grating is discussed in section 5. Conclusions are drawn in section 6.

2. Miniature spectrometer based on diffractive optics

Current state-of-the-art broadband spectrometer devices contain two fully-fledged spectrometers inside a unit or just a separate spectrometer which works either in the visible/near-infrared (VIS/NIR) range or SWIR-infrared (SWIR) range. The current most compact, broadband, robust and low-cost spectrometers are from Avantes, Ocean Optics Hamamatsu, Ibsen Photonics and BAYSPEC [14-18]. The specifications of these miniaturized spectrometers are given in Table 1. Among these compact spectrometers, the AvaSpec-Mini spectrometer of Avantes has the best spectral resolution (1nm) but has the second largest size, next to the BAYSPEC spectrometer family. Even if it is the largest of all compact spectrometers, the BAYSPEC BRZ-VIS-NIR-SWIR spectrometer can cover the widest spectral range (400-1700 nm) using volume phase gratings. Whereas the Pebble VIS spectrometer from Ibsen Photonics has the smallest footprint; its drawback is that it only operates in the VIS spectral range. As seen from Table 1, the size of the Hamamatsu micro-spectrometer is comparable to the Pebble VIS, but its spectral resolution is worse by a factor of 2.5 compared to the Pebble VIS.

Table 1. Specifications of various miniaturized spectrometers from different suppliers [14-18].

Spectrometer name	Spectral range	Resolution	Size	Vendor
AvaSpec-Mini	200 - 1100 nm	1 nm	95 x 68 x 20 mm^3	Avantes
STS VIS	350 -600 nm	1.5 nm	40 x 42 x 24 mm^3	Ocean Optics
STS NIR	650 - 1100 nm	1.5 nm	40 x 42 x 24 mm^3	Ocean Optics
Micro-spectrometer	340 -850 nm	15 nm	20.1x 12.5x10.1 mm^3	Hamamatsu
Pebble VIS	380 -850 nm	6 nm	17 x15x8 mm^3	Ibsen Photonics
BRZ-VIS-NIR	400 -1000 nm	6-8 nm	118x67x34 mm^3	BAYSPEC
BRZ-VIS-NIR-SWIR	400-1700 nm	7-12 nm	118x67x34mm^3	BAYSPEC

The objective of our research is to develop a compact spectrometer based on diffractive optics that combines the functionalities of a UV, VIS-NIR and SWIR spectrometer in a compact housing of typically 1 cubic inch [13]. In our research, we investigate the design of a micro-spectrometer which combines ease of assembly, cost-efficiency and excellent performance in a small size. Our design strategy relies on utilizing the latest developments in digital camera technology with CMOS and InGaAs image sensors together with a reduction of the number of optical components required by function integration. A minimum amount of discrete hardware components ("blocks") is being used and time-consuming mechanical alignment and calibration procedures are taken over by software routines of which the results are stored in

erasable programmable read-only memory (EPROM). Figure 2 gives an overview of the traditional spectrometer technology (left), and the foremost compact possible spectrometer configuration (right), respectively.

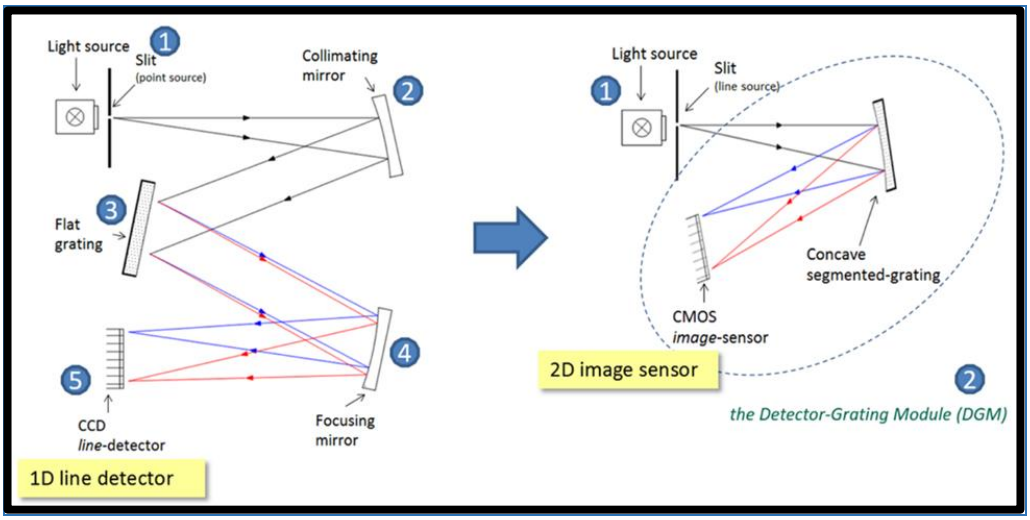

Figure 2. Left - Traditional layout of a spectrometer consisting of five separate components that must be accurately assembled and adjusted: 1) a narrow slit at the input, which serves as a point source, 2) a curved mirror (collimator) that makes the incoming beam parallel, 3) a diffraction grating that deflects the colors of the incoming light at different angles, 4) a curved mirror (focusing mirror) that focuses the color spectrum onto a linear detector, and 5) the linear CCD-detector that converts the color information into electrical signals. Right - The number of components is reduced from five discrete parts to two "blocks" that are simply put together, namely the Detector-Grating-Module (DGM) which is the heart of the spectrometer and the light entrance slit. Precise adjustment and calibration of the spectrometer is done after mechanical assembly with standard image processing software.

The approach of using an integrated module has the advantage of an easier assembly of the instrument. For a compact spectrometer, the mechanical housing and mounting slots for the components could easily be made by precision aluminum extrusion. Once the slots are made, while keeping the required tilt angles in the housing, the components, including the grating, the mirror and detectors could be put in place by sliding them into the premade mounting slots. The spectrometer components (slit, mirror, grating and detector) can tolerate an alignment error of 0.1 mm in their XYZ positions and 1 degree in their XYZ tilt angles without compromising the spectral resolution. Precision aluminum extrusion is able to achieve these tolerance requirements. Sensitivity of the alignment to temperature changes can be ignored as the spectrometer is not intended to be used in extreme weather conditions as the grating is replicated out of polymer. The concept of integrated modules (blocks) can be realized using state-of-the-art two-dimensional CMOS-image sensors readily available from the camera industry combined with a segmented diffraction grating, optimized for the 300 nm to 1700 nm wavelength range. In our case, we didn't use a curved grating configuration yet, but rather a flat segmented grating combined with a collimating and focusing mirror (as shown in Figure 3(b)). By using a segmented grating, we obtain an excellent overall performance of the spectrometer that combines compactness with low cost, a large spectral range and high sensitivity. The miniature spectrometer in our approach consists of three spectrometer segments: a UV (300 nm to 420 nm), VIS-NIR (420 nm to 830 nm) and a SWIR (830 nm to 1700 nm) segment, respectively. The different grating segments are chosen to maximize the overall diffraction efficiency of the spectrometer device.

3. Modelling and design of a compact UV- VIS/NIR-SWIR spectrometer

3.1 Spectrometer configurations

The main goal of the design task is to keep the size of the spectrometer as small as possible while satisfying the required resolution of 6 nm and 10 nm, and SNR of 50 and 150, in the VIS-NIR and SWIR wavelength regions, respectively. Another important design parameter of the spectrometer is the numerical aperture (NA) which affects both its resolution and SNR. A large NA allows the spectrometer to acquire more light (or high throughput) but reduces its resolution due to an increase of optical aberrations. Therefore, the NA should be chosen such that a good balance is obtained between the light throughput and resolution of the spectrometer. The input fiber to the spectrometer is a standard multimode fiber with a core diameter of 200 um and NA of 0.22. Next to the input fiber, there is a slit to control the light throughput and spectral resolution. The smaller the slit, the better the spectral resolution, but the lower the light throughput. That is why a trade-off needs to be made and why we selected a slit width of 25 um. The NA of the micro-spectrometer was chosen to be 0.15 which is less than the NA of 0.22 of the input fiber. As a result, the spectrometer loses 22.34 % of light that could be collected by the fiber (based on equation 1), but its resolution is improved by a factor of 2 (compared to the resolution of a spectrometer with NA of 0.22). For a Gaussian beam, the ratio of the power contained within a radius (r) to the power within the beam waist at any distance (w) (where the intensity drops to 1/e2 of the intensity at the center) is given by equation (1). The numerical aperture is linearly proportional to the beam size, which means that the ratio of the numerical apertures is r/w [19]. The resolution improvement due to lower NA is associated with the lower amount of spherical and field-dependent aberrations of the optical system.

$$Power\ ratio = 1.15 * \left(1 - e^{-2r^2/w^2}\right) = 1.15 * \left(1 - e^{-2*0.15^2/0.2^2}\right) = 77.66\% \qquad (1)$$

We have investigated in detail two basic spectrometer design configurations, namely the Rowland circle and Fastie-Ebert. The Rowland circle configuration consists of a single concave grating whereas the Fastie-Ebert configuration is made up of a flat grating and a spherical mirror. The configurations are schematically shown in Figure 3 (a) and (b), respectively. The two configurations have a relatively small number of components such that a compact spectrometer could be realized.

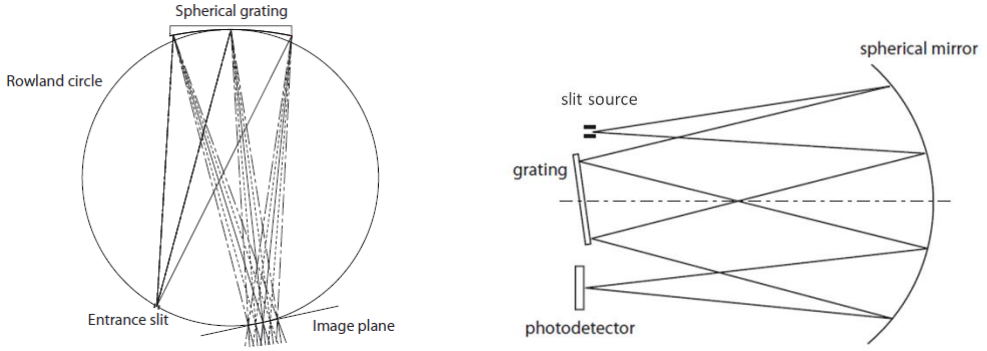

(a) (b)

Figure 3. Two basic configurations for the spectrometer: (a) the Rowland circle configuration with one concave grating, (b) the Fastie-Ebert configuration with a spherical mirror and a flat grating [19].

The Rowland circle configuration has the least number of components but manufacturing the concave grating on a curved profile is very challenging. Therefore, we chose the Fastie-Ebert configuration for our design. Compared to the Rowland circle configuration, the Fastie-Ebert

configuration has one additional mirror, but the grating can be designed and manufactured on a planar surface which strongly eases the challenge of manufacturing. The interesting aspect of the Fastie-Ebert configuration is that coma aberrations can be corrected by the spherical mirror as the light hits the mirror surface twice: firstly, at the top part and secondly at the bottom of the mirror [20, 21].

However, with the classical Fastie-Ebert configuration, there might not be enough space to position all the components (the source (the slit), the grating and the detector) in a small volume. Therefore, this configuration was modified by moving the grating forward with respect to the spherical mirror to create an extra space between the grating and the source on the one hand and the grating and the detector at the other hand. We call this the "open arms configuration". Adapting the classical Fastie-Ebert configuration to an 'open-arm' Fastie-Ebert configuration requires to increase the incidence angle at the mirror and the exit angle (from the mirror to the detector). In this case, the grating is positioned closer to the mirror (compared to the classical Fastie-Ebert configuration) and is tilted to keep the overall size of the spectrometer very compact. The position and the focal length of the mirror do not change, but the tilt angles of the grating and the detector, as well as the distance between the grating and the mirror are optimized to reduce the optical aberrations. As a result, there is no further increase in terms of the optical aberrations compared to the classical Fastie-Ebert configuration (Figure 4 (a)).This configuration was chosen for designing the spectrometer based on a three-segment grating.

3.2 Design of a spectrometer with a three-segment diffraction grating

The dimensions of the designed configuration are shown in Figure 4(a). The radius of curvature of the spherical mirror and the distances between the different components are optimized to achieve the resolution and SNR requirements, and a form factor of about one cubic inch. The root mean square (RMS) spot size is used as a merit function to optimize the system performance in Code V (a ray tracing optical design software). The spectrometer consists of one grating with three segments, i.e. the UV, VIS/NIR and the SWIR segments (see Figure 4(b)). The segments have an equal footprint area, but different geometries as shown in Figure 5 (a). They have the same groove density but different blaze wavelengths, blaze angles and spectral ranges, and as a result they have a different groove height. This allows the multi-segment grating (compared to a single segment grating) to have a higher diffraction efficiency over a broad wavelength range. The blaze wavelengths of the three-segment gratings are chosen to maximize the diffraction efficiency of the grating for the broad spectral range from 300 nm to 1700 nm. The grating is blazed for the -1 diffraction order. Therefore, the other (unwanted) diffraction orders are expected to have low diffraction efficiency. Ray tracing simulations show that the 0^{th} order and the positive diffraction orders diffract away from the detector due to the backward tilt of the grating. The negative diffraction orders can be blocked by using black-painted absorbing baffles which can be placed at the bottom of the detector, and bottom and top of the mirror. The profiles of the three segments are plotted together in Figure 5(b). The parameters of the three grating segments are given in Table 2. The grating is used in reflection mode to achieve a compact spectrometer without sacrificing spectral resolution of the spectrometer.

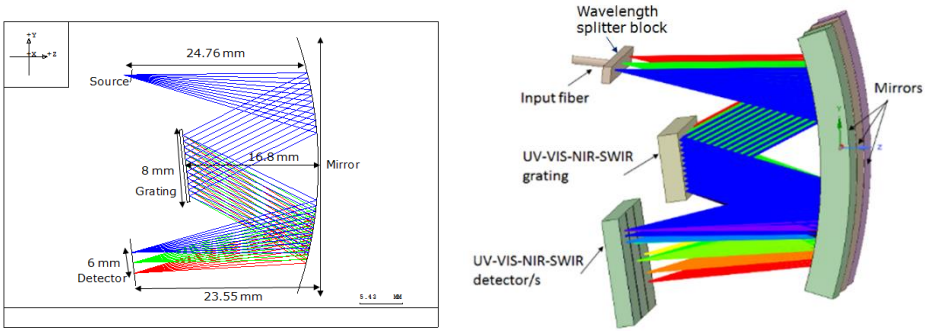

Figure 4. "Open-arms" Fastie-Ebert configuration for the design of the spectrometer. (b) Design of the spectrometer based on a three-segment grating.

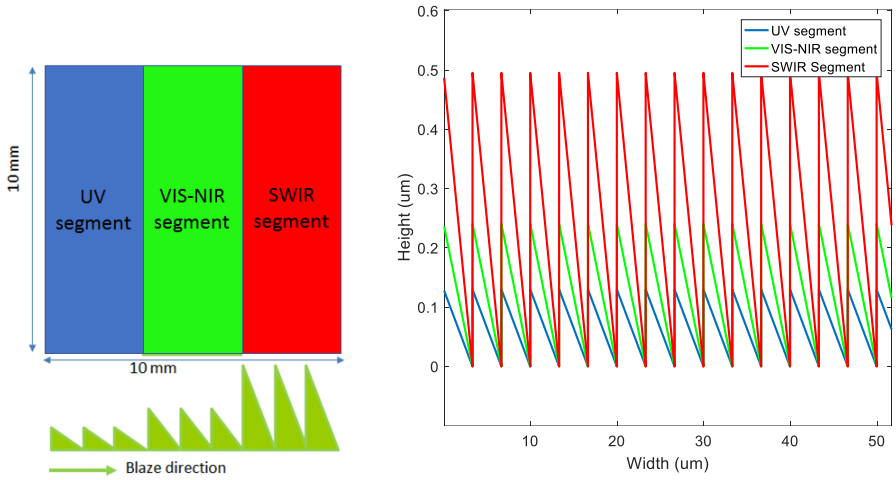

(a) (b)

Figure 5. (a) The footprint of the grating segments and their geometry. (b) The profiles of the three grating segments.

Table 2. Parameters of the three grating segments

Parameters	UV segment	VIS-NIR segment	SWIR segment
Spectral range (nm)	300- 420	420-830	830-1700
Groove density (grooves/mm)	300	300	300
Blaze wavelength (nm)	300	480	980
Blaze angle (°)	2.6	4.1	8.4
Groove height (nm)	149.9	240.6	495.4

4. Performance analysis of the designed spectrometer

4.1 Power budget and sensitivity analysis of the spectrometer

The detection of the signal coming from the tissue under investigation depends on the sensitivity of the spectrometer and the minimum required signal level for the spectral tissue sensing application. The total amount of light available for each wavelength at the detector is determined by several factors. The most prominent factors are the light source spectrum, the spectral absorption and scattering characteristics of the tissue constituents such as water and hemoglobin, the diffraction efficiency of the grating and the detector's spectral response. Moreover, the NA of the spectrometer will also affect the spectrometer throughput. To determine the spectrometer NA, a trade-off between the light throughput and resolution of the spectrometer device needs to be made. For the power budget calculation, we assumed a standard halogen light source. According to health and safety regulations, the total power of the light at the probe end to which the tissue is exposed should not exceed 6 mW [22]. The power of the incident light on the tissue is 5 mW. The absorption characteristics of the tissue constituents such as water determine the amount of light backscattered from the tissue. The backscattered light from the tissue that is collected by the multimode fiber connected to the spectrometer input is about 10^{-4} of the incident light power at the probe end close to the tissue [23]. In addition, we have taken into account the diffraction efficiency of the grating and the quantum efficiency of the detectors. For the UV and VIS/NIR spectrometer a CMOS detector from CMOSIS, i.e., CMV 4000 (2048x2048 pixels, pixel size 5.5 µm) is used [24]. For the SWIR region, an InGaAs linear array (512x1 pixels, pixel pitch 25 µm, pixel height 250 µm) infrared detector is used [25]. As the heights of the CMOS and the InGaAs detectors are similar, they could easily be mounted side by side. In case alignment issues would occur due to the fact that the CMOS and InGaAs detectors have a different width, a blank zone (without grating structure) between the grating segments on the sample could be added to make sure the center of each detector is well aligned with the center of each grating segment. The SNR of the spectrometer is influenced by the absorption characteristics of the tissue, the diffraction efficiency of the grating, the emission spectrum of the light source and the resolution/bandwidth of each spectral region. The SNR of the spectrometer was calculated taking into account all the above parameters and assuming that shot noise is the dominant noise in the system (which means electronic readout noise is for example ignored). An integration time of 200 ms is considered to calculate the SNR for the UV, VIS-NIR and SWIR spectral regions. Therefore, the SNR is equal to the square root of the number of photons/electrons generated in the detector as shown in equation (2).

$$SNR(\lambda, \delta\lambda, \tau) = \sqrt{\frac{P}{\Delta\lambda} \cdot \frac{\lambda}{h \cdot c} \cdot \tau \cdot \delta\lambda \cdot \eta_{scat.} \cdot \eta_{thr} \cdot W_{\lambda} \cdot} \qquad (2)$$

Where λ is the instantaneous wavelength, P is the total power the tissue is exposed (5 mW), $\Delta\lambda$ is the spectral range (which is 1400 nm -from 300 nm to 1700 nm), $\delta\lambda$ is the line width of each wavelength (which is 6 nm in the VIS range and 10 nm in the NIR-SWIR), $\eta_{scat.}$ is the diffused reflectance of the tissue (which is 10^{-4} as given in reference 23), η_{thr} is the light throughput of the system (which is 77% as calculated in equation (1)), W_{λ} is a weighting factor for each wavelength, which represents the cumulative effect of the tissue absorption, the spectral response of the detector, and the diffraction efficiency of the grating, τ is the integration/exposure time of the device (which is taken as 200 ms), and h is Planck's constant (which equals $6.626.10^{-34}$ J s). The SNR of the spectrometer is shown in Figure 6. The minimum SNR calculated in the UV and VIS spectral range is 650, and in the NIR-SWIR it is 9300. These values are significantly larger than the threshold value of the SNR required for spectral tissue sensing which is 50 and 150 in the VIS-NIR and SWIR, respectively. The SNR requirement of

the spectrometer is therefore fulfilled. The SNR in the NIR-SWIR region is higher than in the VIS region because of on the one hand the tissue absorption is higher in the VIS region and on the other hand the emitted power of the halogen source in the VIS region is lower than in the NIR-SWIR region. Moreover, the resolution in the VIS is 6 nm whereas in the SWIR region it is 10 nm, which in turn contributing to the higher SNR in the NIR-SWIR region.

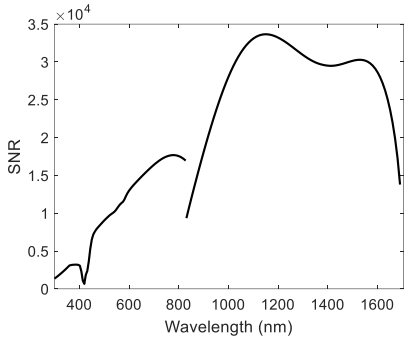

Figure 6. SNR of the spectrometer is higher than the minimum requirement for spectral tissue sensing.

4.2 Irradiance analysis of the spectrometer

The irradiance analysis helps us to evaluate if the resolution requirement of the spectrometer is met or not. The resolution of the spectrometer is determined by the full-width at half-maximum (FWHM) of the irradiance at the detector. The irradiance is used to visualize the distribution of the light over the image sensor of the spectrometer. To do so, the different influencing factors (diffraction efficiency, quantum efficiency of the detectors, tissue absorption) are combined to calculate the weighting coefficients for different wavelengths or the amount of light power received at each pixel.

After performing an irradiance analysis in Code V, we take the cross-section of the detector in the dispersion direction (vertical direction in Figure 7 (a)) to see how the light is distributed over the different wavelengths within the spectral range. For the irradiance analysis we assume that the slit acts as a light source having a Gaussian profile. The slit has a width of 25 µm and height of 200 µm. The source is assumed to have a Gaussian beam profile with a full-width at half -maximum (FWHM) of 200 µm and a NA of 0.15 (corresponding to a divergence half-angle of 11.54º) using a multimode fiber of diameter 200 µm and NA of 0.15 to collect the light scattered from the tissue and bringing it to the input port of the spectrometer. The cross-section of the irradiance is shown in Figure 7(b). We took two wavelengths separated by 6 nm (e.g. 300 nm and 306 nm) for the UV and VIS/NIR spectral range and 10 nm spectral spacing for the SWIR range (1090 nm, 1100 nm…). We then run the irradiance analysis and see if these adjacent wavelengths which are separated by respectively 6 nm (UV and VIS/NIR) and 10 nm (SWIR), are resolved as individual peaks at the detector. The analysis shows that the different colors are well separated, which means they are spectrally resolved. In Figure 7(a) we see separated lines in the different regions of the detector indicating that the 6 nm (UV and VIS/NIR) and 10 nm (SWIR) resolution are achieved. Also, from the cross-sectional plot in Figure 7(b), it is seen that the different peaks are well distinct which assure us that the 6 nm (UV and VIS/NIR) and 10 nm (SWIR) resolution have been achieved with simulation.

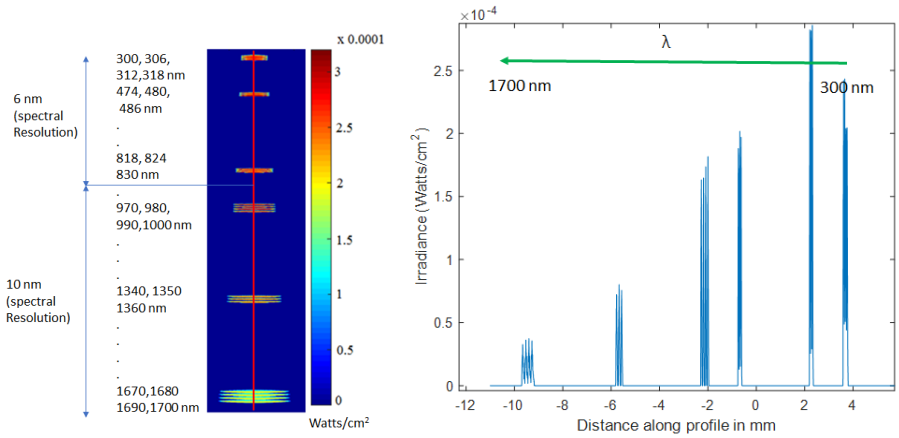

(a) (b)

Figure 7. (a) Irradiance plot for the spectrometer consisting of a three-segment grating operating in the UV, VIS/NIR and SWIR spectral range. The plot shows that wavelengths which are 6 nm (UV and VIS/NIR) and 10 nm (SWIR) apart are well resolved. The color bar shows the irradiance value. (b) Vertical cross-section of the irradiance plot along the red line in Figure 7 (a) shows that the different wavelengths have separated peaks which confirms that they are well resolved.

5. Fabrication of the three-segment diffraction grating and its performance in comparison with a single-segment Richardson grating

5.1 Fabrication of a three-segment diffraction grating and Richardson grating

After the design of the spectrometer and the three-segment grating, we fabricated the grating as well as a single-segment Richardson grating having the same groove density for benchmarking. The Richardson grating and the three-segment gratings were fabricated using the same technology such that a fair comparison of their performances could be made. The reference Richardson grating has 300 grooves/mm and a blaze wavelength of 300 nm [26]. First the grating molds were made in metal using our in-house 5 axis ultraprecision diamond tooling machine [27,28]. The ultraprecision diamond tooling machine is a 350FG from Moore Nanotech. The 5 axes of these machine is shown in Figure 8. A ruling technique is used to make the grating in the mould material which is a Nickel Phosphate (NiP) coated steel. With this technique, the diamond cutting tool is fixed and the workpiece moves vertically in the YZ plane to remove material, thus making the grating profile. In order to control the blaze angle of each segment, the B-axis of the machine is rotated. A diamond tool with an end cutting edge angle of 2°12’ has been used for this ruling process.

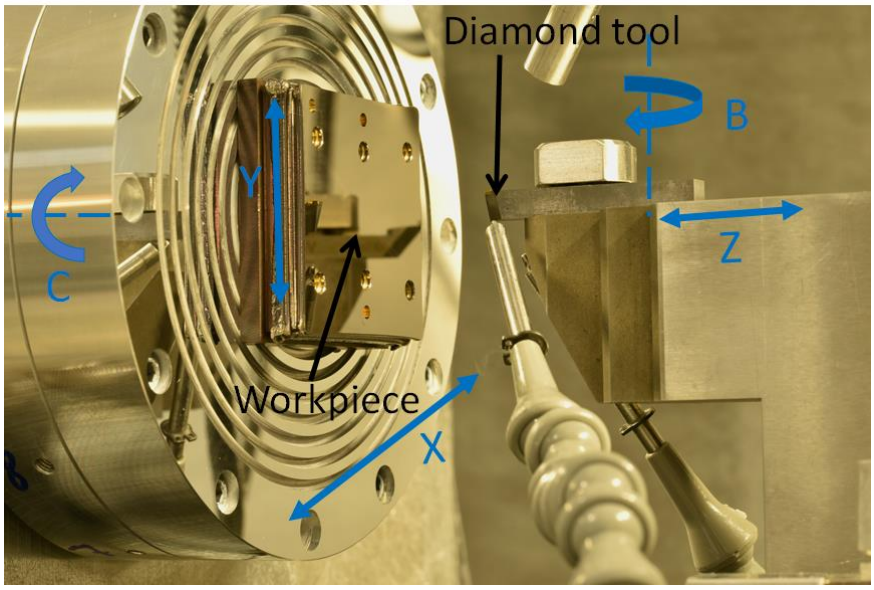

Figure 8. Mould with segmented gratings is made using a 5-axis ultra-precision diamond tooling machine from Moore Nanotech.

Afterwards several copies of the gratings were produced in poly-methyl methacrylate (PMMA) through hot embossing [28]. As the grating is used in reflection mode, a 150 nm gold coating was applied through evaporation. We tried two approaches for coating the grating. The first one consists of applying the gold coating on the PMMA substrate before the hot embossing process. The disadvantage of this approach is that it is difficult to press a mold on a substrate with a thick coating (300 nm) as it requires high pressure which rips off the gold layer during the demolding stage of the hot embossing process. A thick coating is necessary to have high reflectivity for the grating. The second approach is applying the gold coating through sputtering after the grating segments have already been replicated. The problem with this approach is that the sharp edges of the grating become flat and consequently the grating profile becomes sinusoidal instead of triangular. For making the final samples we used the first approach of coating in combination with plasma treatment of the PMMA surface prior to coating. Treating the surface of PMMA with high energy plasma increases adhesion of gold to its surface [29]. After the replication and coating step, the profiles of the fabricated gratings were measured with an atomic microscope (AFM), see Figure 9 (a). The cross-sectional profiles (along the red line in Figure 9 (a)) of the fabricated grating segments and the reference Richardson grating are given in Figure 9 (b). The fabricated grating has an average roughness of 36.6 nm and an RMS roughness of 41.3 nm, when measured over a length of 587nm.

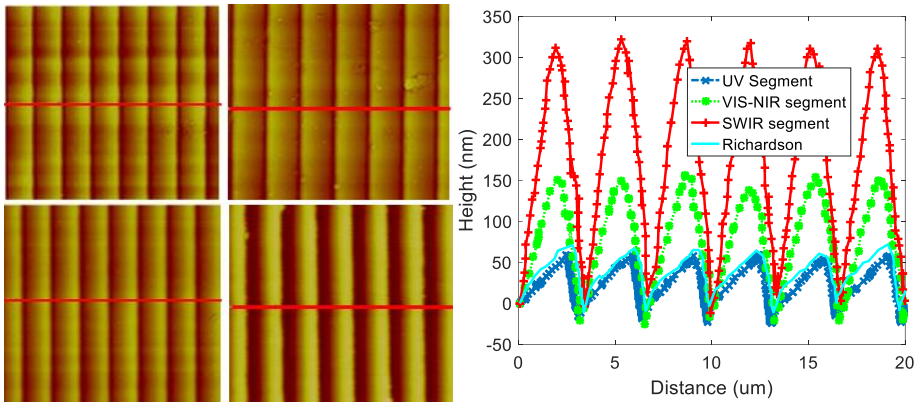

(a) (b)

Figure 9. AFM measurements of the fabricated three-segment grating (a) UV segment (top-left), VIS-NIR segment (top-right), SWIR segment (bottom-right) and Richardson grating (bottom-left). (b) Overlay of the extracted profiles along the cross-sectional line.

5.2 Performance analysis of fabricated diffraction gratings

Once the profiles of the gratings were measured, the measured data were used in VirtualLab (physical optics design software) to evaluate the performance of the fabricated gratings before being tested in a spectrometer setup. Basically, the diffraction efficiency of the fabricated grating with three segments was simulated and compared with that of the single-segment Richardson grating which is used as a benchmark for performance comparison.

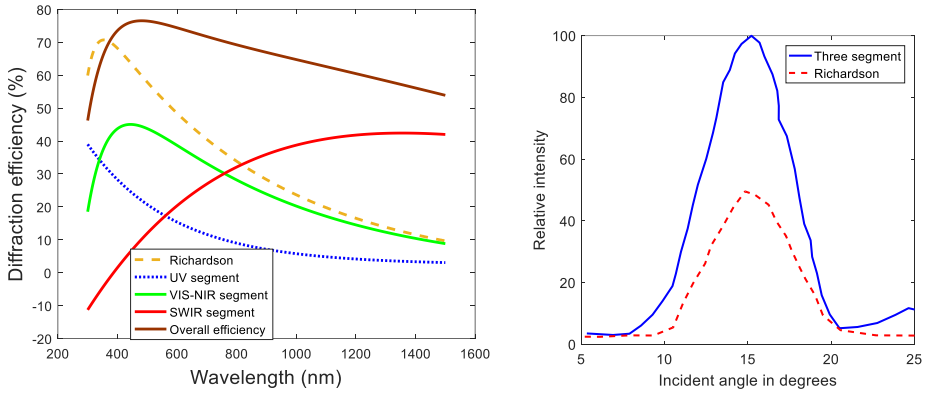

(a) (b)

Figure 10. (a) Simulated diffraction efficiency using the profiles of a fabricated Richardson grating and the fabricated three-segment grating. (b) Measured signal level at wavelength of 900 nm collected by the spectrometer using the three-segment grating and the Richardson grating.

The power received at the detector of the spectrometer is determined by the diffraction efficiency of the diffraction grating and the input power. The grating with the three segments has equal area as the Richardson grating. Therefore, the power received by each segment is one-third of the power received by the Richardson grating (as the area of each segment is one third of the Richardson). Therefore, the overall diffraction efficiency of the three-segment grating is the sum of the diffraction efficiency of the individual segments divided by three. The

overall diffraction efficiency of the three-segment grating is compared with that of the Richardson grating as shown in Figure 10. As seen on Figure 10 (a), the three-segment grating has higher overall diffraction efficiency, especially in the NIR-SWIR regime (as the Richardson grating is blazed at 300 nm). The diffraction efficiency of a spectrometer based on a three-segment grating would be improved by at least a factor of 2 in the NIR and SWIR spectral region compared to a spectrometer based on a Richardson grating. This was further verified in an experiment by inserting the three-segment and Richardson gratings in the standard set-up of the Avantes CompactLine spectrometer and illuminating the grating at different incident angles [30]. The relative received signal level (at a wavelength of 900 nm) with the three-segment grating is about 2 times larger than the Richardson grating at the desired incident angle of 15 degree (which is the incident angle of the light at the grating in the design) (see Figure 10 (b)). For the verification of our three-segment grating, we used a calibration source from Avantes and compared the obtained spectrum with the reference spectrum measured by an Avantes commercial spectrometer (AvaSpec-2048 Starline). The integration time for the measurement was 100 ms. The spectra of the calibration source measured with the commercial and our three-segment grating based spectrometer is given in Figure 11 From Figure 11, it can be seen that the spectrum captured with the three-segment grating based spectrometer clearly follows the spectrum of the calibration source with the commercial spectrometer. In addition, the acquired signal level is even higher compared to the spectrum measured by the AvaSpec-2048 spectrometer. By looking at the details of Figure 11 in the VIS spectral region around 400 nm (see Figure 12 (a)) and in the NIR region around 820 nm (see Figure 12 (b)), it is clear that the 6 nm and 10 nm resolution requirements are achieved. As seen from Figure 12 (both a and b), the achieved resolution in the VIS is even as low as about 3.6 nm and in the NIR region 6 nm. Also the 10 nm resolution requirement in the SWIR region is fulfilled as seen from the signal peaks at 843 and 853 nm in Figure 12 (b). The acquired signal level with the three-segment spectrometer is boosted, which is an indication that the three-segment grating increases the amount of light received by the detector due to that fact that the diffraction efficiency is improved a lot. This is especially clear in the NIR-SWIR spectral region which perfectly agrees with the simulation analysis. Both the simulation and experimental results demonstrate that a three-segment or generally a multi-segment grating can significantly enhance the performance of a spectrometer operating over a broad wavelength range and this allows to develop compact and low-cost spectrometers for different applications such as spectral tissue sensing.

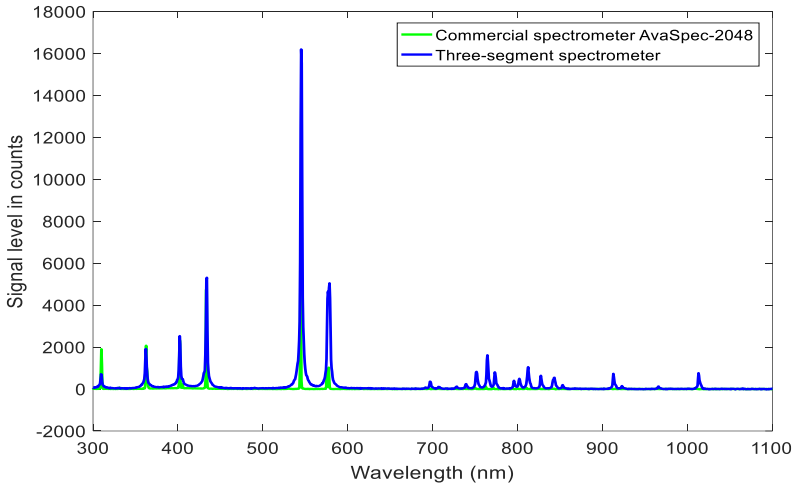

Figure 11. Comparison of the calibration light source spectrum as measured with the three-segment grating based spectrometer (blue) and a commercial spectrometer of Avantes (the AvaSpec-2048 Starline).

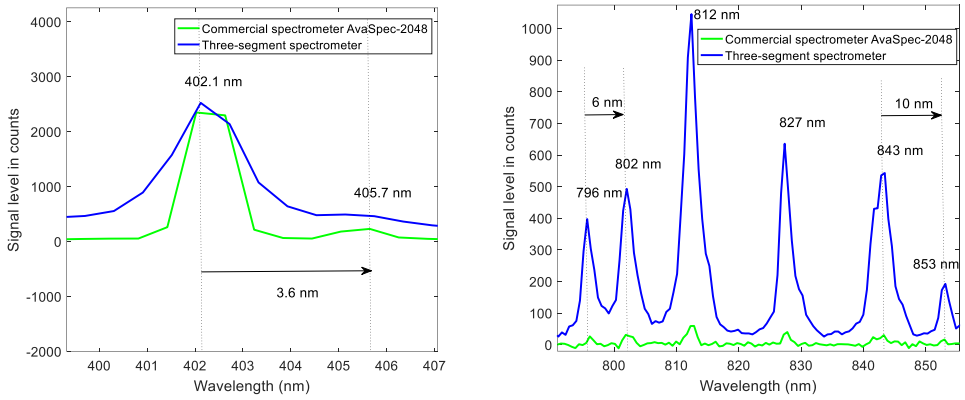

(a) (b)

Figure 12. Detail of the spectrum of Figure 11 with well-resolved peaks indicating that the resolution requirement of 6 nm and 10 nm of the spectrometer is achieved in the (a) VIS region and (b) in the NIR-SWIR region.

6. Conclusion

We have designed a compact three-segment spectrometer which operates in the UV, VIS/NIR and SWIR wavelength range from 300 nm to 1700 nm. The grating segments are blazed to maximize the diffraction efficiency in the broad wavelength range. The spectrometer achieves an SNR of better than 650 in the UV and VIS-NIR, and better than 9300 in the SWIR range, both significantly larger than the threshold of the SNR required for spectral tissue sensing. The spectrometer has a resolution of 6 nm in the UV and VIS/NIR and 10 nm in the SWIR regions. The three-segment grating was fabricated and tested in an experimental set-up. The performance of the three-segment grating was benchmarked with a corresponding single-segment Richardson grating. The three-segment grating improves the signal level acquired by the spectrometer by a factor of 2 in the NIR-SWIR wavelength range. This paves the way towards future compact and yet affordable spectrometers which can operate over a broad spectral range for various point-of-care diagnostic and monitoring applications. Our future endeavors will focus on improving the quality of fabricated gratings through alternative coating mechanisms.

Acknowledgements

The research in this project was funded by the European Union's Horizon2020 research and innovation program under grant agreement "InSPECT - Integrated Spectrometers for Spectral Tissue Sensing", No644483, http://www.inspect2020.eu/. It is a joint project of Philips Research, Philips Healthcare, Vrije Universiteit Brussel (VUB), Anteryon, Xenics, Avantes, XiO Photonics, Fraunhofer IZM and Aifotec. This work was also supported in part by FWO, the Methusalem and Hercules foundations and the OZR of the Vrije Universiteit Brussel (VUB).

References

[1]. Balthasar, A., Desjardins, A.E., Van der Voort, M., Lucassen, G., Roggeveen, S., Wang, K., Bierhoff, W., Kessels, A.G., Sommer, M., and Van Kleef, M., "Optical detection of vascular penetration during nerve blocks: an in vivo human study," Reg Anesth Pain Med 37(1), 3-7 (2012).

[2]. Balthasar, A., Desjardins, A.E., Van der Voort, M., Lucassen, G., Roggeveen, S., Wang, K., Bierhoff, W., Kessels, A.G., Van Kleef, M., and Sommer, M., "Optical detection of peripheral nerves: an in vivo human study," Reg Anesth Pain Med 37(3), 277-282 (2012).
[3]. Desjardins, A.E., Hendriks, B.H., Van der Voort, M., Nachabe, R., Bierhoff, W., Braun, G., Babic, D., Rathmell, J.P., Holmin, S., Soderman, M. and Holmstrom, B., "Epidural needle with embedded optical fibres for spectroscopic differentiation of tissue: ex vivo feasibility study," Biomed Opt Express 2(6), 1452-1461 (2011).
[4]. Desjardins, A.E., Van der Voort, M., Roggeveen, S., Lucassen, G., Bierhoff, W., Hendriks, B.H., Brynolf, M., and Holmstrom, B. "Needle stylet with integrated optical fibres for spectroscopic contrast during peripheral nerve blocks", J Biomed Opt 16(7), 077004 (2011).
[5]. Nachabe, R., Hendriks, B.H., Desjardins, A.E, Van der Voort, M., Van der Mark, M.B., and Sterenborg, H.J., "Estimation of lipid and water concentrations in scattering media with diffuse optical spectroscopy from 900 to 1600 nm", J Biomed Opt 15(3),037015 (2010).
[6]. Bodanese B., Silveira, F.L., Zângaro, R.A., Pacheco, M.T., Pasqualucci, C.A., Silveira, L.,"Discrimination of basal cell carcinoma and melanoma from normal skin biopsies in vitro through Raman spectroscopy and principal component analysis" Jr., Photomed Laser Surg. 30(7), 381-7 (2012).
[7]. Brancaleon, L., Durkin, A.J, Tu, J.H., Menaker, G., Fallon, J.D., Kollias, N., "In vivo fluorescence spectroscopy of nonmelanoma skin cancer", Photochem Photobiol.73(2), 178-83 (2001).
[8]. Ramanujam, N., Brown, J., Bydlon, T.M., Kennedy, S.A., Richards, L.M., Junker, M.K., Gallagher, J., Barry, W.T., Wilke, L.G., Geradts, J., "Quantitative spectral reflectance imaging device for intraoperative breast tumor margin assessment", Conf Proc IEEE Eng Med Biol Soc. 2009:6554-6 (2009).
[9]. Nayak, S., Blumenfeld, N. R., Laksanasopin, T., and Sia, S. K., "Point-of-Care Diagnostics: Recent Developments in a Connected Age," *Analytical Chemistry* 89(1), 102-123 (2017).
[10]. Wilson, R.H., Nadeau, K.P., Jaworski, F.B., Tromberg, B.J. and Durkin, A.J., "Review of short-wave infrared spectroscopy and imaging methods for biological tissue characterization", Journal of Biomedical Optics 20(3), 030901 (2015).
[11]. Evers, D.J., Nachabe, R., Vranken Peeters, M. J., van der Hage, J. A, Oldenburg, H. S., Rutgers, E.J., Lucassen, G. W., Hendriks, B. H., Wesseling, J., Ruers, T. J., "Diffuse Reflectance Spectroscopy: Towards Clinical Application in Breast Cancer." Breast Cancer Research and Treatment 137 (1), 155–65 (2013)
[12]. Evers, D.J., Nachabe, R., Hompes, D., Van Coevorden, F., Lucassen, G. W., Hendriks, B. H , Van Velthuysen, M. L.F. , Wesseling, J., and Ruers, T. J.M., "Optical Sensing for Tumor Detection in the Liver." European Journal of Surgical Oncology 39 (1), 68–75 (2013).
[13]. "InSPECT", http://www.inspect2020.eu/.
[14]. "AvaSpec-Mini spectrometer", ttps://www.avantes.com/products/spectrometers/compactline/item/1236-avaspec-mini-cl.
[15]. "Ocean Optics spectrometer STS series", https://oceanoptics.com/product-category/sts-series/
[16]. "Hamamatsu micro-spectrometer", http://www. Hamamatsu .com/eu/en/product/category/5001/4016/C12880 MA/index.html.
[17]. "Pebble VIS, ultra-compact cost-efficient OEM spectrometer modules for the visible range", https://ibsen.com/products/oem-spectrometers/pebble-spectrometers/pebble-vis/
[18]. "Breeze™ – Smart Palm Spectrometer", https://www.bayspec.com/spectroscopy/breeze-smart-palm-spectrometer/
[19]. "Gaussian beam optics, technical note", https://www.newport.com/n/gaussian-beam-optics.
[20]. Grabarnik, S., "Optical microspectrometers using imaging diffraction gratings", Master Thesis, University of Delft, ISBN: 978-90-9025048-9 (2010).
[21]. Palmer, C., Loewen, E., *Diffraction Grating Handbook* (sixth ed.), Newport Corporation (2005).
[22]. Biosafety standards IEC 60601-2-57 and EN 60601-2-57.
[23]. Jacques, S.L., "Optical properties of biological tissues: a review," Phys. Med. Biol. 58, R37–R61 (2013)
[24]. "CMV 4000 area scan sensors", http://www.cmosis.com/products/product_detail/cmv4000
[25]. "Xlin detector series," http://www.xenics.com/en/xlin-detector-series.
[26]. "Ruled diffraction gratings with blaze angle 2.5 degree and 300 grooves per mm," http://www.gratinglab.com/Products/Product_Tables/Efficiency/Efficiency.aspx?catalog=53-*-090R
[27]. Belay, G. Y., Ottevaere, H., Meuret, Y., Vervaeke, M., Erps, J. V., and Thienpont, H.,"Demonstration of a multichannel, multiresolution imaging system, " Appl. Opt. 52, 6081-6089 (2013).
[28]. J. Van Erps, M. Vervaeke, F. Duerr, and H.Thienpont, "Prototyping and Replication of Polymer Freeform Optical Components ," OSA Optical Fabrication and Testing (2017).
[29]. Uba, F. I., Pullagurla, S. R., Sirasunthorn, N., Wu, J., Park, S., Chantiwas, R., Cho, Y.K,Shin, H., Soper, S. A. "Surface charge, electroosmotic flow and DNA extension in chemically modified thermoplastic nanoslits and nanochannels," The Analyst, 140(1), 113–126 (2015).
[30]. "AvaSpec-Mini4096CL", https://www.avantes.com/products/spectrometers/compactline/item/1390-avaspec-mini-cl.